

A Brain-inspired Embodied Intelligence for Fluid and Fast Reflexive Robotics Control

Weiyu Guo^{1,4}, He Zhang^{1,4}, Pengteng Li^{1,4}, Tiefu Cai^{1,4}, Ziyang Chen^{1,4}, Yandong Guo^{1,4}, He Xiao⁴, Yongkui Yang^{3*}, Ying Sun^{1,2*}, and Hui Xiong^{1,2*}

¹The Thrust of Artificial Intelligence, The Hong Kong University of Science and Technology (Guangzhou), Guangzhou, China.

²The Department of Computer Science and Engineering, The Hong Kong University of Science and Technology, Hong Kong, China

³Shenzhen Institutes of Advanced Technology, Chinese Academy of Sciences, Shenzhen, China

⁴AI² Robotics, Shenzhen, China

*The corresponding authors (yk.yang@siat.ac.cn, zhuhengshu@gmail.com, xionghui@ust.hk).

ABSTRACT

Recent advances in embodied intelligence have leveraged massive scaling of data and model parameters to master natural-language command following and multi-task control. In contrast, biological systems demonstrate an innate ability to acquire skills rapidly from sparse experience. Crucially, current robotic policies struggle to replicate the dynamic stability, reflexive responsiveness, and temporal memory inherent in biological motion. Here we present Neuromorphic Vision-Language-Action (NeuroVLA), a framework that mimics the structural organization of the bio-nervous system between the cortex, cerebellum, and spinal cord. We adopt a system-level bio-inspired design: a high-level model plans goals, an adaptive cerebellum module stabilizes motion using high-frequency sensors feedback, and a bio-inspired spinal layer executes lightning-fast actions generation. NeuroVLA represents the first deployment of a neuromorphic VLA on physical robotics, achieving state-of-the-art performance. We observe the emergence of biological motor characteristics without additional data or special guidance: it stops the shaking in robotic arms, saves significant energy (only 0.4w on Neuromorphic Processor), shows temporal memory ability and triggers safety reflexes in less than 20 milliseconds.

1 Introduction

The pursuit of general-purpose embodied intelligence has been accelerated by Vision-Language-Action (VLA) models, which unify perception, reasoning, and actuation to master complex tasks^{1,2}. However, current architectures remain far from matching the adaptive motor intelligence inherent in humans and animals. First, restricted to current-step visual observations, these architectures suffer from temporal blindness, failing to perceive execution progress in repetitive tasks. Second, their inability to process high-frequency signals and lack of proprioceptive feedback result in severe action jitter and failure to reflex instantaneously in dynamic scenarios. Ultimately, invoking a large foundation model for every fine-grained motor adjustment incurs prohibitive power consumption and extreme computational inefficiency.

To resolve this bottleneck, we look to biological motor intelligence, which achieves robustness not through a monolithic processor, but via a hierarchical division of labor. Contemporary theories of optimal feedback control posit that biological agility relies on a distinct hierarchical architecture of sensorimotor loops to overcome the intrinsic latencies of neural transmission^{3,4}. Rather than centralized micromanagement, the nervous system enforces a strict functional partitioning: (1) Cortical regions integrate multisensory streams to generate semantic goals and high-level plans; (2) the cerebellum, receiving dense sensorimotor inputs, acts as a high-frequency adaptive module that predicts sensory consequences, refines motor commands, and contributes critically to temporal memory and error correction^{5,6}; and (3) the spinal cord comprises interneuronal networks and reflex pathways that realize fast, decentralized sensorimotor loops⁷. This architectural separation decouples semantic planning from high-frequency proprioceptive modulation and execution and underpins smooth trajectories, rapid protective responses, and energy-efficient behavior, supporting the lifelong plasticity of low-level motor circuits⁸.

We validate this architecture across simulated benchmarks and physical robotic hardware, demonstrating capabilities that are difficult to replicate via existing tokenized sequence-modeling paradigms (e.g., VLAs). Experimental results indicated that functions akin to biological motor intelligence emerged in the model, even in the absence of pre-training data or specific supervision. First, the cerebellar module functions as a critical adaptive damper: by acting as an effective filter, it suppresses high-frequency intention tremor to reduce kinematic jerk by over 75% and anchors execution in proprioceptive states. This

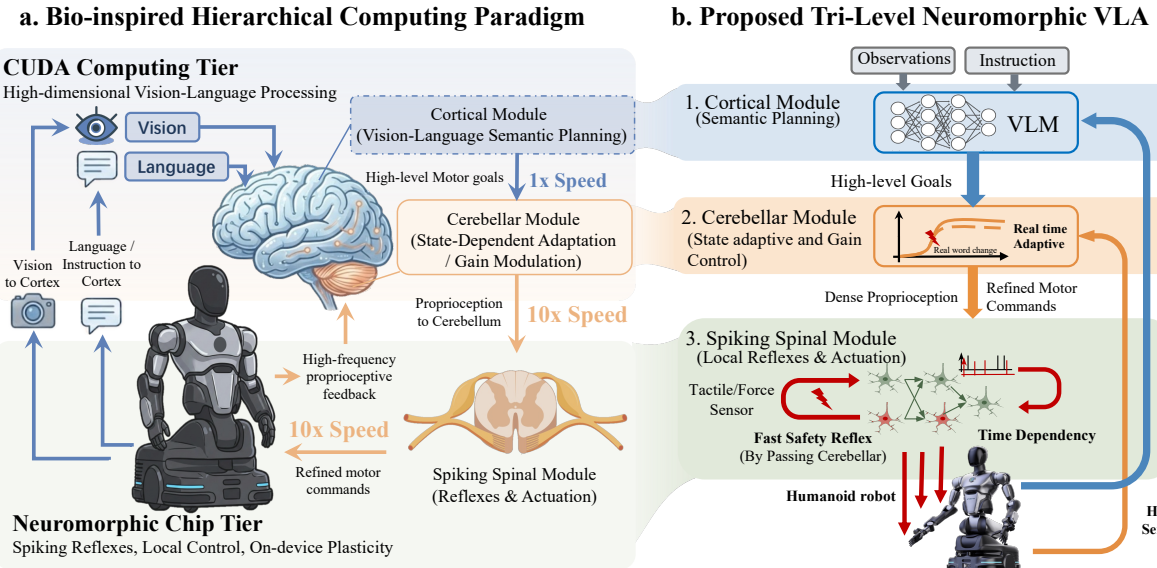


Figure 1. Hierarchical decoupling of semantic planning and neuromorphic motor control. a, The Bio-inspired Computing Paradigm bridges the timescale gap between cognition and actuation. The architecture allocates high-latency, high-dimensional visual-language processing to a **CUDA Computing Tier (Cortical Module)**, while offloading high-frequency proprioceptive modulation and reflexes to an energy-efficient **Neuromorphic Chip Tier (Cerebellar/Spinal Modules)**. This separation enables a $10\times$ speedup in local sensorimotor loops compared to cortical planning. **b**, Data flow in the **Tri-Level Neuromorphic VLA**. (1) The **Cortical Module** synthesizes abstract, low-frequency motor goals from visual instructions. (2) The **Cerebellar Module** functions as a state-adaptive filter, utilizing dense proprioception to perform real-time gain modulation (inset graph), compensating for dynamic discrepancies. (3) The **Spiking Spinal Module** translates these commands into precise actuation via Spiking Neural Networks (SNNs). Crucially, it incorporates a **Fast Safety Reflex** pathway (red loop) that processes tactile/force signals locally to trigger withdrawal responses, bypassing the slower cortical loop entirely, while enabling on-device plasticity for continuous adaptation.

ensures smooth execution essential for fine-grained manipulation and maintains temporal rhythmicity—anticipating task phases rather than purely reacting—even in the presence of noisy visual feedback. Moreover, the neuromorphic spinal layer exhibits functional self-organization characteristic of biological circuits. We observe two complementary forms of sparsity that were not explicitly supervised: temporal sparsity, where neurons spontaneously revert to quiescence during static posturing to minimize metabolic cost; and spatial disentanglement, where the network naturally segregates high-dimensional control signals into distinct, somatotopic behavioral modes. Crucially, this event-driven substrate enables survival capabilities inaccessible to conventional planners. Under unexpected physical collisions, the cerebellar module leverages force feedback to trigger rapid (< 20 ms) withdrawal reflexes via cerebellar-spinal loops, bypassing the prohibitive latency (> 200 ms) of the cortical loop⁹. To test the capability for rapid few-shot learning, we eschewed massive expert datasets. Instead, we utilized only the pretrained weights of a Vision-Language Model (VLM) and fine-tuned on a limited set of a few hundred downstream samples, remarkably achieving task success rates that even outperformed the pretrained baselines.

Our findings demonstrate that mimicking the hierarchical architecture of the biological motor nervous system endows robots with highly adaptive and energy-efficient embodied intelligence. Rather than introducing brittle complexity¹⁰, this bio-inspired hierarchy reduces control overhead by decoupling functionalities across circuits commensurate with their intrinsic timescales and physiological roles. Consequently, the proposed architecture offers a scalable computational scaffold for future embodied agents, ensuring that high-level semantics and low-level reflexes operate in parallel to achieve robust and fluid performance.

2 Results

2.1 A Bio-inspired VLA with Event-driven Sparsity

To reconcile the conflicting timescales of semantic cognition and high-frequency actuation, we instantiated the biological motor hierarchy within a distributed computational framework: Neuromorphic Vision-Language-Action (NeuroVLA) architecture (Fig. 1). This system fundamentally decouples the CUDA Computing Tier, responsible for latency-tolerant semantic reasoning, from the Neuromorphic Chip Tier, dedicated to millisecond-level sensorimotor loops.

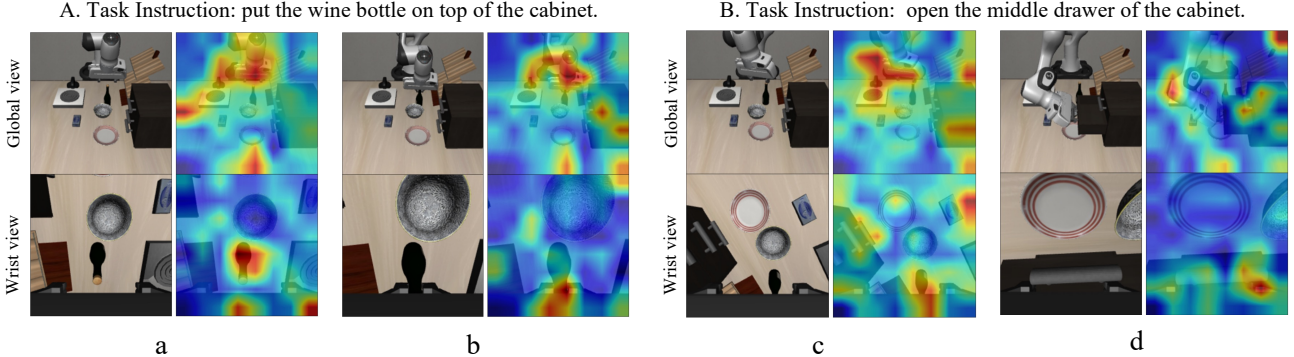


Figure 2. Semantic distillation of descending motor intent via attentional gating. Analogous to the **corticospinal tract**, which filters high-dimensional cortical processing into streamlined execution commands, the Q-Former interface extracts task-specific geometric features while suppressing task-irrelevant information. **a, b**, Multi-stage intent extraction for the task “Put the wine bottle on the cabinet.” The mechanism initially isolates the manipulation target (wine bottle) in the wrist view to guide grasping (**a**), before shifting attention to the destination surface to orchestrate placement (**b**), mirroring the sequential focus of motor planning. **c, d**, Semantic selectivity under the instruction “Open the middle drawer.” Despite the visual salience of the wine bottle (a potential distractor), the descending queries actively inhibit this feature (**c**), instead exclusively grounding the drawer handle (**d**). This confirms that the module does not merely encode visual saliency but performs top-down attentional modulation, ensuring that only task-relevant spatial primitives are transmitted to downstream cerebellar and spinal circuits.

At the cortical level, the CUDA tier processes computationally heavy visual and linguistic modalities. To bridge the dimensionality gap between high-level reasoning and low-level control, we employ a Querying Transformer (Q-Former) structure¹¹. Functionally analogous to biological descending motor pathways (e.g., the corticospinal tract) which distill complex cortical dynamics into streamlined motor commands, the Q-Former extracts compact, task-relevant intention signals from the dense VLM representations. These distilled low-frequency signals are transmitted to the Neuromorphic tier, where the Cerebellar Module acts as an adaptive filter. By ingesting high-frequency proprioceptive and force signals—which significantly outpace visual frame rates—this module serves a dual role: it smooths kinematic trajectories via gain control and provides robust resistance to visual sensory noise, enabling rapid trajectory re-planning without waiting for cortical updates¹².

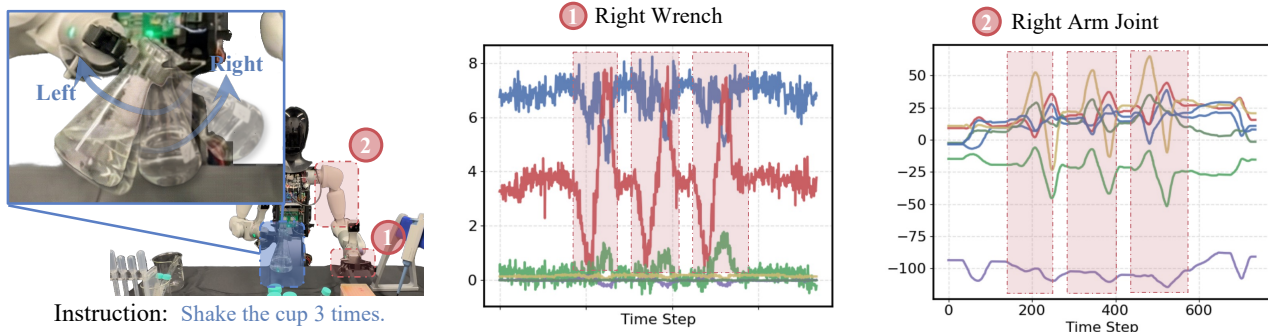
The hierarchy is grounded in the Spiking Spinal Module, deployed on the neuromorphic hardware to enforce extreme metabolic efficiency. Deviating from the dense computations of standard deep learning, this module exploits the event-driven sparsity of Spiking Neural Networks (SNNs). Neurons are selectively recruited only during active kinematic changes, with firing rates dropping to near-quiescence during static holding phases, thereby minimizing power consumption while maintaining vigilance. Moreover, unlike stateless Multi-Layer Perceptron (MLP) heads that treat control as independent regression steps, the intrinsic membrane dynamics of the spinal SNN naturally encode temporal dependencies. This preserves motion continuity and enables fast, monosynaptic-like safety reflexes, strictly mirroring the physiological division of labor. Further details of the methods are provided in Method 4.

2.2 Task intent drives top-down attentional gating of spatial primitives

To investigate how abstract semantic goals are translated into actionable motor commands, we visualized the cross-modal attention maps generated by the Intention Extraction Module (Fig. 2). We observed a distinct dynamic reconfiguration of spatial attention conditioned solely on linguistic instructions, overriding bottom-up visual saliency. In scenes populated with multiple potential interactors (e.g., a wine bottle and a cabinet drawer), the system exhibited precise attentional selectivity that dynamically evolves/shifts in alignment with task progression. Under the instruction “Put the wine bottle on top of the cabinet” (Fig. 2a-b), the descending queries formed a preferential attachment to the bottle’s geometry, effectively filtering out the adjacent drawer despite its visual prominence. Subsequently, as the task advanced to the placement phase, the focus seamlessly shifted to the target destination. Crucially, when the instruction was switched to “Open the middle drawer” (Fig. 2c-d) within the identical visual scene, the attentional hotspot shifted instantaneously to ground the drawer handle, effectively filtering out visually prominent but irrelevant distractors.

These observations indicate that the module functions as an active semantic filter. Rather than passively encoding the entire scene, the system implements a top-down attentional spotlight that isolates task-relevant geometric primitives while suppressing perceptual entropy. This mechanism creates a semantic information bottleneck functionally isomorphic to the biological *corticospinal tract*, ensuring that downstream cerebellar and spinal circuits receive only the streamlined, task-essential execution commands necessary for low-latency control.

a. Temporal Sensorimotor Dynamics as a Compact Form of Motor Memory



b. Collision-Induced Wrench Perturbations and Cerebellum-Inspired Trajectory Adjustment

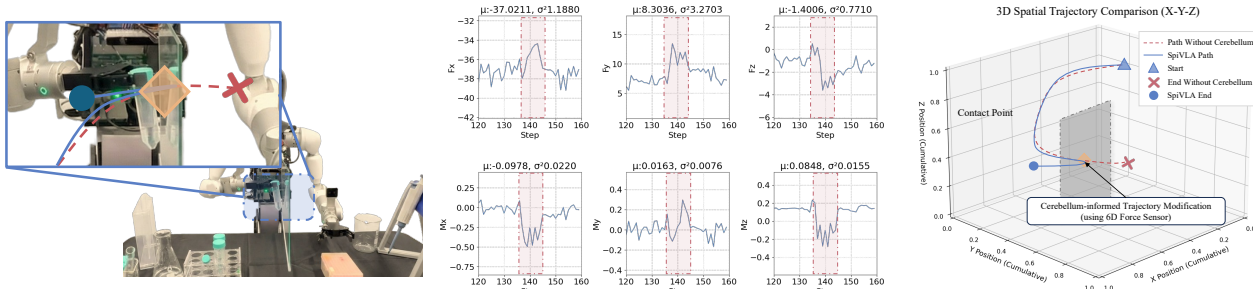


Figure 3. Proprioceptive temporal dynamics and force-aware adaptive control. **a**, Temporal sensorimotor dynamics as a compact form of motor memory. In rhythmic manipulation tasks (e.g., “Shake the cup”), the system encodes the motion primitive not through redundant visual frames, but via high-frequency trajectories of **Right Wrench** (force/torque) and **Right Arm Joint** states. This proprioceptive encoding allows the agent to maintain phase consistency and temporal rhythm independent of visual occlusion. **b**, Collision-induced wrench perturbations and cerebellum-inspired trajectory adjustment. Real-time monitoring of 6D wrench signals detects a physical contact event (sharp spike in force profiles). Upon detection, the cerebellar feedback loop triggers an immediate spatial trajectory reformulation (blue solid line in 3D plot), allowing the end-effector to autonomously navigate around the obstacle, whereas the open-loop baseline (red dashed line) fails to adapt.

2.3 The cerebellar module recapitulates the three canonical functional loops of the biological cerebellum

To investigate the mechanistic basis of the system’s robustness, we analyzed the agent’s behavior under diverse physical conditions. Our observations suggest that the Cerebellar Module does not merely act as a generic filter, but functionally instantiates the three distinct phylogenetic loops of the biological cerebellum: the *Spinocerebellum*, *Vestibulocerebellum*, and *Cerebrocerebellum*.

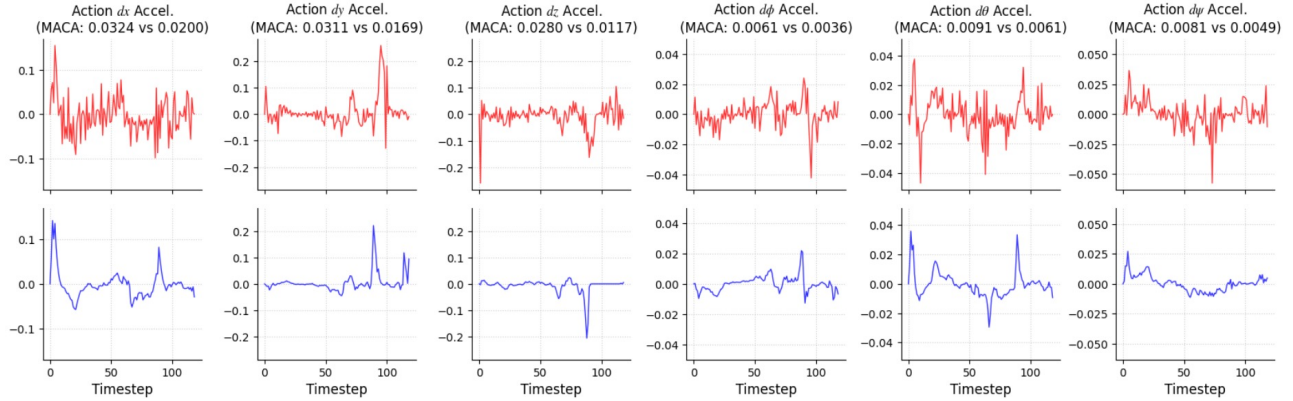
Spinocerebellar loop: Damping intention tremor via proprioceptive gain control

We first examined the kinematic stability of the robotic arm during free-space motion. As visualized in the acceleration traces (Fig. 4a), the baseline cortical policy (the red line) exhibited significant high-frequency stochastic oscillations across all spatial dimensions, a phenomenon mechanistically analogous to “clinical intention tremor.” However, upon activating the cerebellar loop, we observed a suppression of these oscillations (the blue line). Quantitative analysis confirms that the module leverages real-time proprioceptive feedback (joint angles and velocities) to continuously compute the discrepancy between predicted and observed states, attenuating motion jerk by an average of 75.6% (peaking at 80.2% in Δ yaw and 80.0% in Δ Z) relative to the baseline (Fig. 4b). Consequently, this smoothing effect leads to a significant reduction in the Mean Absolute Commanded Acceleration (MACA) by 32.8% to 58.0% across all axes (Fig. 4c). These results indicate that the module effectively recapitulates the *Spinocerebellum* (Paleocerebellum) function: it regulates digital “muscle tone” to dampen execution noise and smooth trajectories, independent of the high-level semantic planner.

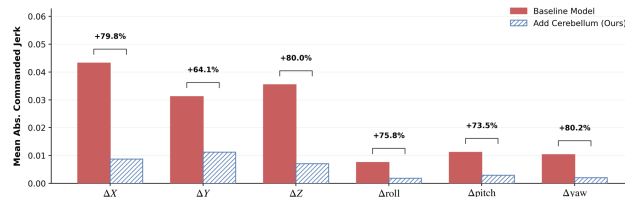
Vestibulocerebellar loop: Restoring equilibrium via fast force reflexes

Next, we assessed the system’s capacity to maintain physical equilibrium under perturbation. In the collision experiments (Fig. 3b), we observed distinct signatures in the high-frequency sensor data: physical contact manifested as sharp, immediate spikes in the 6-DoF wrench profile (middle panel). Specifically, the impact induced high-magnitude fluctuations, with force

a. Cerebellum Module Significantly Reduces Robotic Arm Jitter (Action Commanded Acceleration Comparison)



b. Mean absolute Jerk of Actions



c. Mean absolute Acceleration of Actions

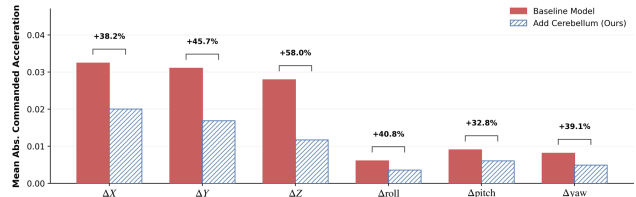


Figure 4. Cerebellar-mediated attenuation of high-frequency kinematic motor noise. a, Qualitative comparison of commanded acceleration traces over time. The baseline cortical policy (red) exhibits significant high-frequency stochastic jitter (analogous to “intention tremor”) across translation (dx, dy, dz) and rotation ($d\phi, d\theta, d\psi$) dimensions. The inclusion of the cerebellar module (blue) acts as a physiological damper, producing markedly smoother control signals. **b, c,** Quantitative assessment of kinematic smoothing. Bar charts show the **b**, Mean Absolute Commanded Jerk and **c**, Mean Absolute Commanded Acceleration. The cerebellar module achieves substantial noise attenuation, reducing average jerk by over 75% and average acceleration by over 40% compared to the monolithic baseline, confirming its critical role in stabilizing stochastic cortical outputs prior to spinal execution.

readings surging to mean values of $\mu \approx -37.02$ in F_x and $\mu \approx 8.30$ in F_y , accompanied by significant variances (e.g., $\sigma^2 \approx 3.27$ in F_y) indicative of sudden instability. While the vision-centric baseline—constrained by high inference latency—persisted in executing the blocked plan (red dashed line), our system exploited these sparse, high-frequency (> 200 Hz) force signals to detect the anomaly within milliseconds. Consequently, the agent triggered an instantaneous spatial trajectory reformulation (blue solid line), successfully navigating around the obstacle. This emergent behavior confirms that the 6-DoF force sensor acts as a functional vestibular organ. By bypassing the slow cortical loop to trigger local corrective actions, the system instantiates a *Vestibulocerebellum*-like (Archicerebellum) reflex, preserving operational “postural stability” and equipment safety through rapid, local adaptation.

Cerebrocerebellar loop: Encoding temporal rhythm as motor memory

Finally, we investigated the representation of complex, rhythmic manipulation tasks. In the “Shake the cup” protocol (Fig. 3a), we observed that the motion primitive was encoded not as a sequence of redundant visual frames, but as a structured periodic trajectory. As detailed in the sensorimotor traces, the semantic instruction was directly translated into three distinct, high-fidelity oscillatory cycles (red shaded regions). The 6-DoF wrench profile (middle panel) and joint angles (right panel) exhibited precise temporal synchronization, with the sinusoidal joint modulations perfectly aligning with the force feedback dynamics across all three repetitions. This proprioceptive encoding allowed the system to maintain phase consistency and rhythmicity even when visual feedback was static or occluded. In the meantime, as shown in Fig. 5e, comparative analysis under sensory degradation revealed that while cortical baselines faltered when lighting or textures were altered, the cerebellar-enhanced agent maintained high success rates by leveraging the invariance of physical dynamics. This observation suggests that the module performs cross-modal sensory re-weighting to serve as a robust form of motor memory. Mirroring the *Cerebrocerebellum* (Neocerebellum) and the dentate nucleus, the system decouples temporal sequencing from visual perception, effectively “immunizing” the agent against environmental entropy and visual sensory failure.

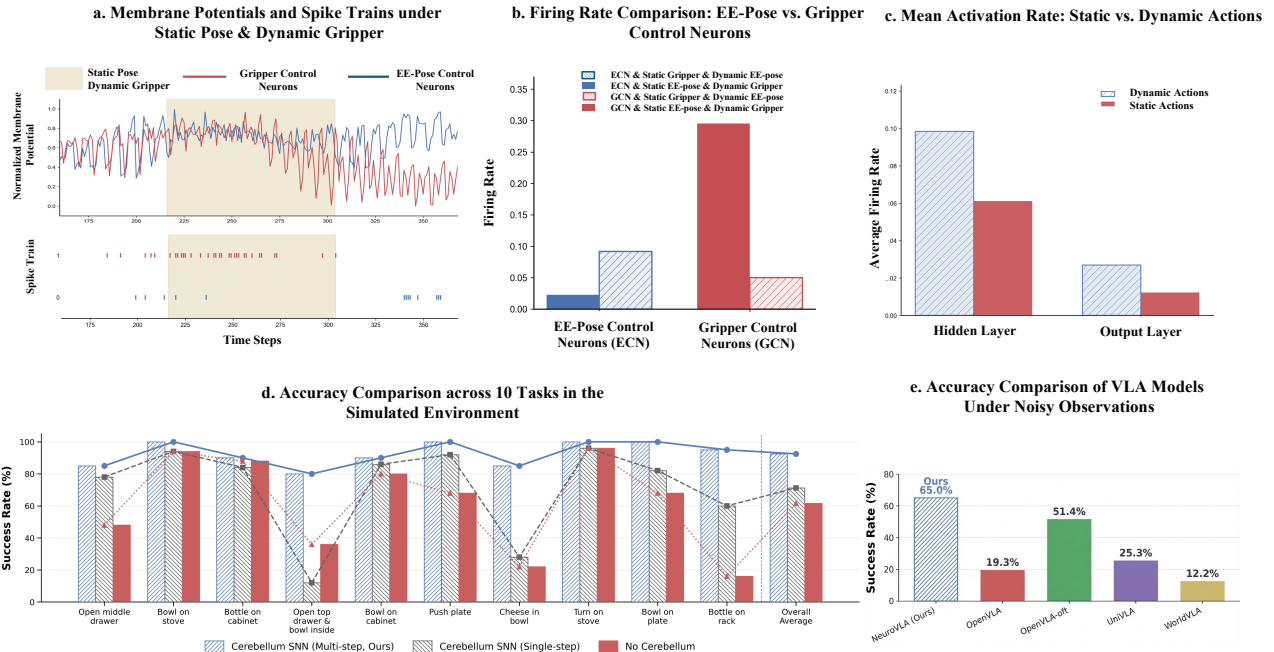


Figure 5. Event-driven sparsity and temporal robustness of the neuromorphic spinal module. **a, b**, Selective neural recruitment and functional modularity. **a**, Traces of membrane potentials and spike trains demonstrate the event-driven nature of the SNN. During the specific phase of “Static Pose & Dynamic Gripper” (shaded region), the **Gripper Control Neurons (GCN, red)** exhibit high-frequency spiking activity driven by the actuation demand, while the **End-Effectuator Pose Control Neurons (ECN, blue)** remain relatively quiescent. **b**, Quantitative comparison of firing rates confirms this decoupling: neurons are selectively recruited only when their corresponding motor primitives undergo state changes, minimizing redundant computation. **c**, Metabolic efficiency via temporal sparsity. Mean activation rates across network layers drop significantly during static holding phases compared to dynamic action phases. This “activity-on-demand” mechanism ensures low power consumption, crucial for edge-side deployment on battery-constrained robots. **d**, Ablation study on the LIBERO benchmark. The **Multi-step SNN** (blue), which integrates temporal context, consistently outperforms the **Single-step SNN** (red) and the **No-Cerebellum baseline** (green). The performance gap is particularly pronounced in long-horizon tasks (e.g., “Bowl on stove”), validating that the spinal module’s intrinsic temporal dynamics—analogous to the cerebellum’s role in sequencing—are essential for robust complex manipulation.

2.4 Event-driven sparsity and temporal integration in the neuromorphic spinal substrate

Having established the role of the cerebellar loop in modulation, we next validated the computational efficiency of the Spiking Spinal Module, which functions as the system’s execution interface. Biological spinal circuits are characterized by extreme metabolic efficiency, recruiting motor neurons only when actuation is demanded. Our neuromorphic implementation strictly adheres to this principle of event-driven sparsity. As visualized in the membrane potential traces (Fig. 5a), the network exhibits a profound functional decoupling: during phases of “Static Pose & Dynamic Gripper,” neurons controlling the end-effector pose remain in a sub-threshold, quiescent state, while gripper-specific neurons burst into high-frequency spiking activity. This selective recruitment is quantified in Fig. 5b, confirming that the architecture avoids the wasteful, continuous computation characteristic of standard Artificial Neural Networks (ANNs). Consequently, the mean activation rate drops significantly during static holding phases (Fig. 5c), effectively implementing an “activity-on-demand” energy profile that is critical for prolonged deployment on battery-constrained Neuromorphic hardware.

Beyond metabolic benefits, the spinal SNN plays a decisive role in temporal information processing. Unlike standard stateless policies that treat sequential control as independent Markovian steps, spiking neurons possess intrinsic memory via membrane potential leakage and accumulation¹⁴. This creates a natural temporal receptive field. We assessed this capability on the LIBERO^{18,31} benchmark (Fig. 5d), comparing our Multi-step SNN against a Single-step variant (ablation of temporal integration) and a No-Cerebellum baseline. The Multi-step SNN achieved superior success rates, particularly in long-horizon tasks requiring phase transitions (e.g., “Bowl on stove”). The performance degradation observed in the Single-step variant suggests that the temporal integration inherent to the spiking dynamics serves as a short-term working memory, essential for preserving motion continuity and logic across extended manipulation sequences. Thus, the spinal module is not merely a passive actuator, but an active, spatiotemporal computer that harmonizes energy efficiency with control robustness.

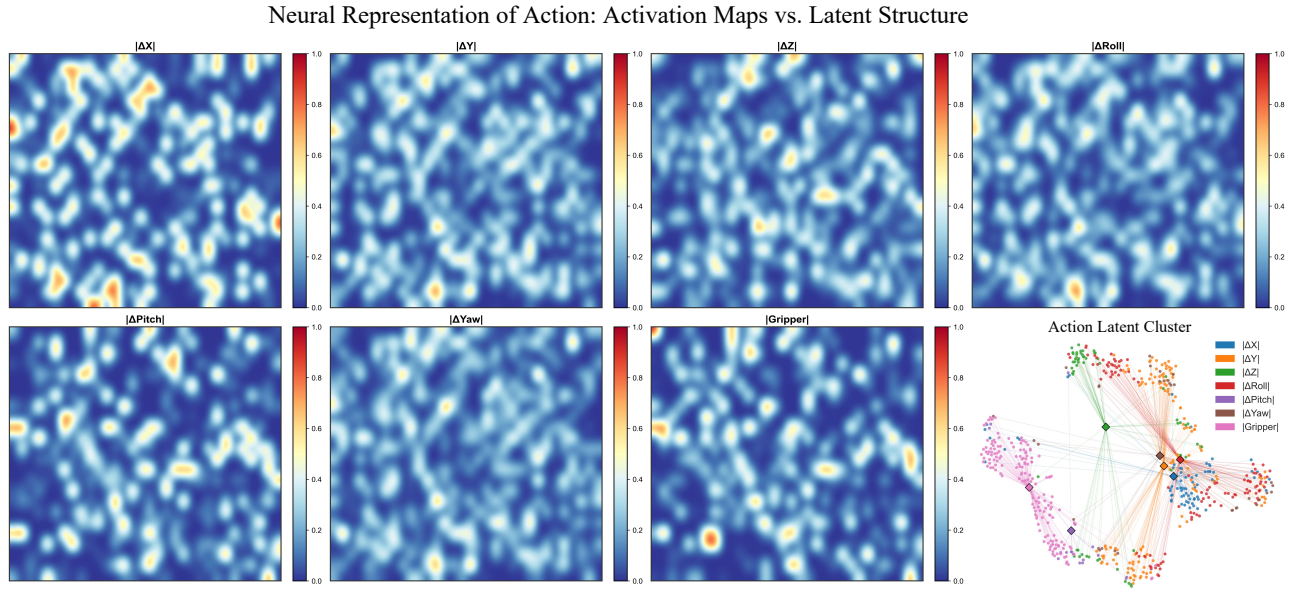


Figure 6. Emergent functional specialization and latent disentanglement in the neuromorphic spinal substrate. **Neural Representation of Action:** Spatially rearranged firing rate maps reveal a spontaneous functional organization where distinct neural subpopulations are selectively recruited to encode specific kinematic dimensions (e.g., $|\Delta Roll|$ vs. $|\text{Gripper}|$), mirroring the energy-efficient modularity of the biological motor cortex. **Action Latent Cluster:** the low-dimensional t-SNE projection of spinal hidden states demonstrates the network’s intrinsic capacity to disentangle high-dimensional control signals into discretely clustered behavioral modes (motor primitives) without explicit supervision, validating the emergence of structural representation learning.

The visualization (Fig. 6 Neural Representation of Action) shows the mean firing rates of neurons in the first hidden spiking layer, spatially rearranged to highlight topological structure. Each map represents the neural population response conditioned on a dominant kinematic dimension (e.g., $|\Delta Z|$, $|\text{Gripper}|$), with red indicating high metabolic activity. The distinct, non-overlapping activation patterns across dimensions reveal a spontaneous somatotopic organization, where specific neural subpopulations are selectively recruited to control specific Degrees of Freedom (DoF), mirroring the functional segregation found in the biological motor cortex. (Fig. 6 Action Latent Cluster) depicts the low-dimensional manifold structure of the spinal hidden states projected via t-SNE. The clear separation of color-coded motor primitives (e.g., green for vertical ΔZ motion, pink for Gripper actuation) demonstrates that the spiking network disentangles high-dimensional control signals into distinct behavioral modes without explicit supervision, validating the network’s internal capacity for structural representation learning.

2.5 Neuromorphic processor validation confirms the spinal module’s low latency and energy efficiency.

The Spiking Spinal Module is deployed on a customized neuromorphic processor which is implemented on an FPGA platform (Fig. 7a). To minimize inference latency, the design adopts a systolic-array architecture (Fig. 7b) that offers high spatio-temporal parallelism while reducing data movement. Spatial parallelism is achieved by updating multiple LIF²⁴ neurons concurrently across array columns with spike reuse, whereas temporal parallelism arises from parallel weight accumulation along array rows with weight reuse. This organization markedly accelerates computation compared with conventional neuromorphic processors—such as IBM’s TrueNorth²⁵ and Intel’s Loihi²⁶—whose neuron updates proceed in a time-sequential fashion. To further improve energy efficiency, a spike-detection module enables spike-sparsity-aware computation by suppressing inactive events: spikes that remain non-active throughout the entire time window are prevented from entering the systolic array, thereby eliminating unnecessary neuron updates^{35,36}. The FPGA hardware resource utilization and the performance summary are presented (Fig. 7c-d), respectively. At an operating frequency of 20 MHz, the design achieves an inference latency of 2.19 ms and an energy cost of 0.87 mJ per inference.

2.6 Real-world Observations of Emergent Motor Intelligence

To validate the ecological validity of the NeuroVLA beyond simulation, we deployed the architecture on a physical bimanual humanoid platform performing a suite of biochemical protocols (Fig. 8a). These tasks were selected to probe distinct motor primitives: spatial precision (relocating test tubes), dynamic fluid control (pouring), and rhythmic sequencing (flask shaking).

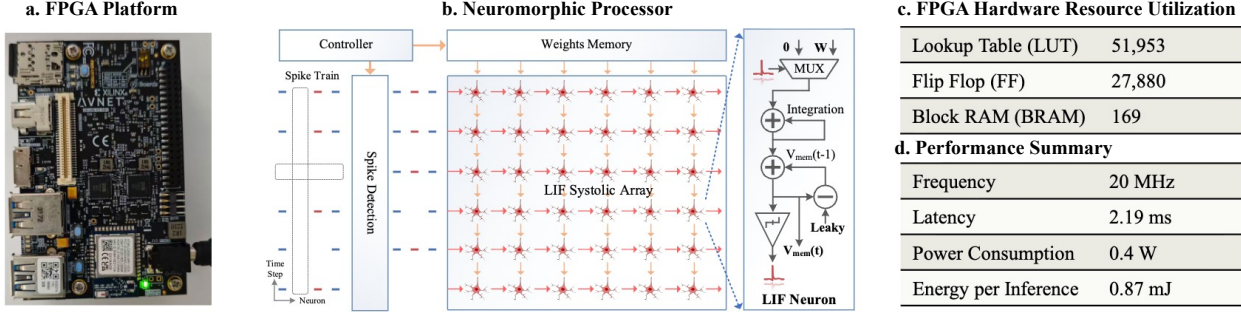


Figure 7. Neuromorphic processor implemented on an FPGA platform for deploying the Spiking Spinal Module. **a**, FPGA board used for implementation. **b**, Neuromorphic processor incorporating an LIF systolic-array architecture and spike-sparsity-aware computation to reduce inference latency and energy consumption. **c**, FPGA resource utilization, with 51,953 LUTs, 27,880 FFs and 169 BRAMs. **d**, Performance summary, showing an inference latency of 2.19 ms at 20 MHz and an energy cost of 0.87 mJ per inference.

As detailed in (Fig. 8b–f), our system consistently outperformed state-of-the-art monolithic baselines, including OpenVLA², OpenVLA-OFT¹⁵, UniVLA¹⁷ and WorldVLA¹⁶. The performance gap was particularly pronounced in tasks involving fine manipulation and fluid dynamics. For instance, during liquid pouring (Fig. 8c), monolithic models frequently suffered from open-loop drift; once the pouring vessel tilted, the visual occlusion of the liquid level and the non-linear weight shifts caused these models to overshoot or spill. In contrast, the NeuroVLA leveraged the Cerebellar Module to integrate high-frequency proprioceptive feedback (200 Hz), allowing it to sense the shifting center of mass and modulate wrist gain in real-time, thereby maintaining a smooth, spill-free trajectory despite visual uncertainty. Similarly, in rhythmic tasks like flask shaking (Fig. 8e), the Spinal Module’s intrinsic temporal memory maintained phase consistency, whereas baseline models often exhibited jerky, aperiodic motions due to their inability to encode high-frequency temporal dependencies.

However, the most profound evidence of emergent intelligence was observed under safety-critical perturbations. We introduced a “Recover to Safe Area” stress test (Fig. 8g), where the robot encounters an unmodeled physical obstruction while handling fragile glassware—a scenario representative of unstructured environments. Here, standard cortical-centric VLAs suffered catastrophic failure (0.0% success rate). The failure mode was consistent: constrained not merely by the latency of the vision-language inference loop (> 200 ms), but fundamentally by the structural absence of specialized modules for high-frequency proprioceptive processing, these models failed to register the instantaneous collision force until deep into the contact event, typically persisting in executing the blocked plan until mechanical stall or object breakage.

In stark contrast, our system achieved a 54.8% recovery rate, demonstrating emergent survival behaviors. This capability is mechanically attributable to the decoupling of perception and survival. Upon detecting a sudden wrench spike via 6-DoF sensors, the neuromorphic spinal substrate triggers a monosynaptic-like withdrawal reflex (< 50 ms latency). This fast-path response bypasses the slower cortical planner entirely, retracting the end-effector to prevent damage. Crucially, this is not a hard-coded stop; following the reflex, the Cerebellar Module utilizes the tactile feedback to orchestrate a local trajectory reformulation, guiding the arm around the obstacle to resume the task. This result provides empirical confirmation that robust embodied intelligence requires a division of labor: a cortical “brain” for semantic intent, supported by a spinal “body” capable of handling the immediacy and unpredictability of the physical world.

3 Discussion

Reinstating the Biological Hierarchy in Embodied AI

Current approaches to embodied intelligence have largely focused on scaling monolithic Vision-Language-Action models, implicitly assuming that motor control will emerge as a byproduct of semantic pre-training. Our results challenge this assumption. We demonstrate that while cortical-scale models excel at high-level planning, they suffer from inherent latency and open-loop drift when directly tasked with high-frequency actuation. By instantiating a bio-inspired Neuromorphic Architecture, we show that the path to robust embodied agents lies not merely in data volume, but in reinstating the architectural inductive biases selected by evolution: a distinct separation of semantic planning, state modulation, and action execution.

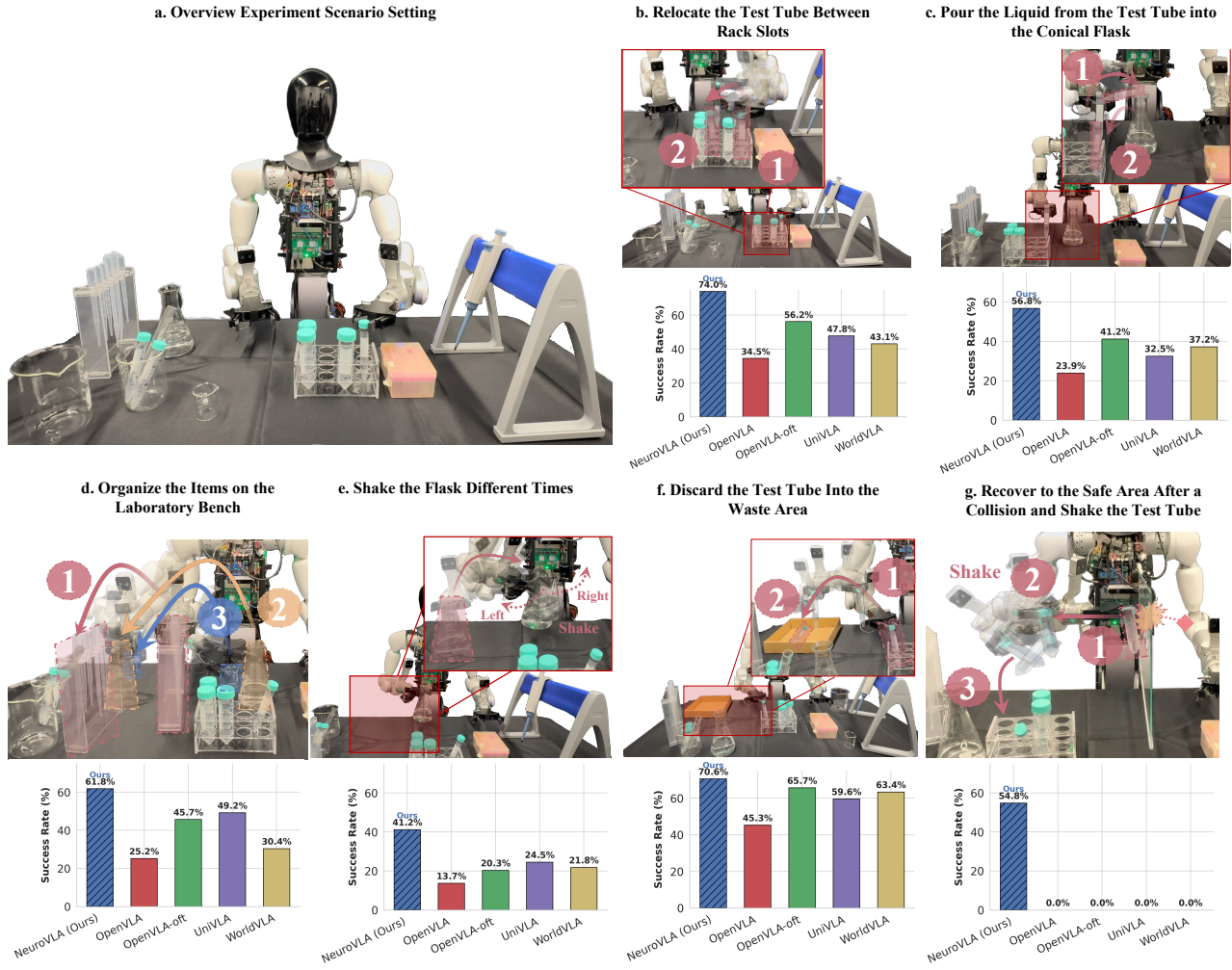


Figure 8. Versatile manipulation dexterity and safety-critical adaptation in physical laboratory environments. **a–e**, Performance on standard manipulation tasks. The proposed NeuroVLA (blue bars) consistently outperforms state-of-the-art VLA baselines (OpenVLA, OpenVLA-OFT, UniVLA, WorldVLA) across tasks demanding spatial precision (**a**, relocating test tubes; **c**, organizing items; **e**, discarding waste), dynamic trajectory smoothness (**b**, pouring liquid), and temporal rhythmicity (**d**, shaking flasks). The results highlight the architecture’s capability to handle complex contact dynamics and long-horizon sequencing. **f**, Safety-critical collision recovery. In this stress test, the robot encounters an unexpected physical obstruction while holding a fragile test tube. Baseline models, lacking low-level reflex circuits, suffer catastrophic failure (0.0% success rate). In contrast, the NeuroVLA detects the contact force via the spinal module, triggers a rapid withdrawal reflex, and autonomously re-plans to navigate around the obstacle and complete the shaking task, demonstrating emergent survival behaviors in unstructured environments.

The Neuromorphic Advantage

The integration of the *Spinal Module* marks a paradigm shift from continuous-time computing to event-driven neuromorphic control. Our analysis of the spinal SNN reveals two critical advantages. **Metabolic Parsimony**: by adhering to the principle of activity-on-demand, the system drastically reduces computational redundancy during static holding phases (Fig. 5a), offering a viable path for deploying complex policies on battery-constrained edge hardware. **Temporal Dependence**: Unlike standard stateless MLPs that generate discrete actions or action chunks, the stateful membrane dynamics of our LIF neurons explicitly capture temporal dependencies. This intrinsic integration converts stochastic neural spikes into continuous action commands (Fig. 4), effectively bridging the gap between the discrete SNN or MLP and the continuous nature of physics.

Reflexes: Survival Precedes Understanding

We achieve rapid reflexes through the simulation of cerebellum and spinal cord structures—essential for dynamic physical interaction. Traditional VLA systems treat collision avoidance as a planning problem, constrained by the latency of visual

perception. Our Safety Reflex experiments (Fig. 8g) demonstrate that survival behaviors should be decoupled from semantic reasoning. The success of our cerebellum module in triggering monosynaptic-like withdrawal reflexes (< 20 ms) proves that **survival precedes understanding**. By bypassing the cortical bottleneck, we endow the robot with a physiological intuition for physical pain, ensuring safety even when the high-level planner is confused or occluded.

Limitations and Future Outlook

While we observe the emergence of some biological intelligence capabilities in our work, current limitations point to future research directions. First, our SNN training relies on GPU acceleration with surrogate gradients; Realizing the full energy-efficiency potential will require training deployment on specialized neuromorphic chips (e.g., Loihi or Tianjic²⁹). Second, the current learning rule relies on offline behavior cloning; incorporating online Spike-Timing-Dependent Plasticity (STDP) could enable true lifelong learning, allowing the spinal module to adapt to muscle fatigue or wear over time. Ultimately, NeuroVLA exhibits emergent biological motor functions by simulating the hierarchical organization of biological motor systems. This provides a novel perspective for VLA design, suggesting that future research should look beyond data to uncover the latent potential within biological neural structures.

4 Methods

4.1 Architecture Overview

We formalize the embodied control task as a Partially Observable Markov Decision Process (POMDP)³⁰. At each time step t , the agent receives a multimodal observation tuple $o_t \in \mathcal{O}$, comprising high-dimensional visual sensory data $I_t \in \mathbb{R}^{H \times W \times 3}$, a natural language instruction L , and a history of low-dimensional proprioceptive states $\mathbf{s}_{t-H:t} \in \mathbb{R}^{H \times D_s}$, where H denotes the size of history window and D_s represents the dimensions of joint positions, velocities, and end-effector forces (6-DoF wrench). The objective is to generate a sequence of continuous motor actions $\mathbf{a}_t \in \mathcal{A}$ to maximize the cumulative reward.

To reconcile the conflicting computational requirements of semantic planning (high-latency, abstract) and motor execution (low-latency, precise), we propose the **Tri-Level Neuromorphic Vision-Language-Action (NeuroVLA)** architecture. As shown in Fig. 1, the system control policy $\pi(a_t|o_t)$ is decomposed into a hierarchical composition of three specialized mapping functions:

$$\mathbf{a}_t = \Phi_{\text{spine}}(\Phi_{\text{cerebellum}}(\Phi_{\text{cortex}}(I_t, L), \mathbf{h}_t)),$$

where Φ_{cortex} , $\Phi_{\text{cerebellum}}$, and Φ_{spine} correspond to the cortical, cerebellar, and spinal modules, respectively. \mathbf{h}_t denotes the compact dynamic context vector from the neurological state estimator. This decomposition enforces a strict division of labor across timescales and hardware substrates:

1. **Cortical Semantic Projection (Φ_{cortex})**: Operates on the CUDA Computing Tier. It maps the visual-linguistic inputs (I_t, L) into a semantic latent intention space $\mathbf{z}_{\text{sem}} \in \mathbb{R}^{D_{\text{model}}}$, where D_{model} denotes the dimension of model internal feature space. This module utilizes a Vision-Language Model (VLM) backbone to extract open-vocabulary affordances, unaffected by high-frequency physical perturbations.
2. **Cerebellar State Modulation ($\Phi_{\text{cerebellum}}$)**: Operates on the CUDA Computing Tier. It functions as a state-dependent affine transformation. A recurrent estimator aggregates the proprioceptive history $\mathbf{s}_{t-H:t}$ into a dynamic context vector \mathbf{h}_t . This context is then used to modulate the semantic latent \mathbf{z}_{sem} via a Gated Feature-wise Linear Modulation (FiLM) mechanism, yielding a refined, physics-aware latent code \mathbf{z}_{mod} . This process mimics the biological cerebellum's role in gain control and error correction based on the efference copy and sensory feedback.
3. **Spinal Neuromorphic Decoding (Φ_{spine})**: Operates on Neuromorphic Chip Tier. It maps the modulated latent \mathbf{z}_{mod} to continuous actions \mathbf{a}_t via a Spiking Neural Network (SNN) governed by Leaky Integrate-and-Fire (LIF) dynamics. This module leverages event-driven sparsity and intrinsic temporal memory to ensure energy-efficient, smooth trajectory generation and rapid reflex responses.

The entire system is trained end-to-end using a hybrid objective that combines behavior cloning losses with surrogate gradients²² for the non-differentiable spiking components, ensuring functional coherence across the hierarchy.

4.2 Cortical Module: Semantic Latent Generation

The Cortical Module occupies the highest tier of the control hierarchy, tasked with cross-modal reasoning and the synthesis of abstract motor intentions from high-dimensional observations. Unlike lower-level circuits that must react to instantaneous physical dynamics, the cortical layer operates on a semantic timescale, prioritizing long-horizon planning and generalization over high-frequency control.

4.2.1 Vision-Language Reasoning Backbone

We leverage a pre-trained Large Vision-Language Model (VLM), specifically Qwen-VL²⁷, as the general-purpose reasoning engine. Formally, given the current RGB observation I_t and the natural language instruction L , the VLM functions as a dense feature extractor:

$$\mathcal{H}_t = F_{\text{VLM}}(I_t, L; \theta_{\text{vlm}}),$$

where $\mathcal{H}_t = \{h_t^{(1)}, \dots, h_t^{(N)}\}$ represents the stack of hidden states across all N transformer layers and θ_{vlm} denotes the parameters of VLM. This rich representation encapsulates scene geometry, object semantics, and linguistic understanding, providing a “world model” necessary for open-vocabulary reasoning and manipulation.

4.2.2 Layer-wise Semantic Distillation

Directly feeding the high-dimensional, variable-length VLM hidden states into a motor policy is computationally prohibitive and prone to overfitting. To bridge the dimensionality gap between the VLM’s linguistic-visual space and the robot’s control manifold, we employ a **Layer-wise Querying Transformer (Q-Former)**.

The Q-Former acts as a learnable information bottleneck. It utilizes a set of learnable query tokens $\mathbf{Q} \in \mathbb{R}^{K \times D}$ to attend to specific subsets of the VLM’s hidden representations, where K denotes the number of tokens and D denotes the token dimension. Crucially, rather than utilizing only the final layer, we extract features from a designated range of intermediate layer index $[l_{\text{start}}, l_{\text{end}}]$ to capture both low-level spatial details and high-level semantic abstractions. The extraction process is formalized as:

$$\mathbf{z}_{\text{sem}} = \text{Q-Former}(\text{Concat}(\mathcal{H}_t[l_{\text{start}} : l_{\text{end}}]), \mathbf{Q}; \theta_{\text{Q-Former}}),$$

where $\mathbf{z}_{\text{sem}} \in \mathbb{R}^{K \times D_{\text{action}}}$ denotes the **Semantic Latent Intention** and $\theta_{\text{Q-Former}}$ denotes the parameters of Q-Former.

Biological Insight: This mechanism mirrors the biological principle of *cortical abstraction*. Just as the brain’s motor cortex sends compact, population-level intent signals (rather than raw pixel data) to downstream circuits, our Q-Former distills the VLM’s vast knowledge into a compact, action-centric representation. This semantic latent \mathbf{z}_{sem} encodes “*what to do*” (e.g., grasp the cup) while remaining agnostic to the specific physics of “*how to do it*” (e.g., compensate for friction), effectively decoupling semantic planning from physical modulation.

4.3 Cerebellar Module: Gated Recurrent Neuromodulation

While the cortical module generates semantic intentions, it operates significantly slower than the dynamics of physical interaction and lacks access to high-frequency proprioceptive feedback. To bridge this gap, the Cerebellar Module functions as an adaptive filter, performing *dynamic state estimation* and *trajectory refinement* before the signals reach the spinal execution layer.

4.3.1 Proprioceptive State Estimation via Recurrent Dynamics

Biological motor control relies on the spinocerebellar tract to convey real-time information about limb position, velocity, and external forces. To model this, we employ a Gated Recurrent Unit (GRU)²⁸ as a neurological state estimator. Let $\mathbf{s}_{t-H:t} \in \mathbb{R}^{H \times D_s}$ denote the history of robot states over a horizon H (aligned with the sensor frequency, e.g., 50 Hz), where each state vector includes joint angles, velocities, and 6-DoF wrench measurements. The estimator integrates this temporal sequence to produce a compact dynamic context vector \mathbf{h}_t :

$$\mathbf{h}_t = \text{GRU}(\mathbf{s}_{t-H:t}; \theta_{\text{gru}}),$$

where θ_{gru} denotes the parameter of the designed GRU. Unlike static encoders (e.g., MLPs), the GRU captures the *rate of change* and *contact transients* (e.g., collision impulses), which are critical for stabilizing motion under perturbation.

4.3.2 Gated Feature-wise Linear Modulation (FiLM)

The core computational role of the cerebellum is to modulate cortical commands based on current physical constraints. We formalize this interaction using a Gated FiLM mechanism²³. First, to prevent proprioceptive noise from overwhelming semantic intent during stable phases, we employ a learnable gating factor \mathbf{g}_t :

$$\mathbf{g}_t = \sigma(W_g \cdot \text{Proj}(\mathbf{h}_t)),$$

where σ , W_g and $\text{Proj}(\cdot)$ denote the sigmoid function, the learnable affine transformation matrix and the projection function. This gate selectively regulates how much physical context is allowed to influence the cortical plan. Subsequently, the dynamic context \mathbf{h}_t is projected into affine transformation parameters—scale γ_t and shift β_t —which are applied to the cortical semantic latent \mathbf{z}_{sem} :

$$\gamma_t = f_\gamma(\mathbf{h}_t), \quad \beta_t = f_\beta(\mathbf{h}_t)$$

$$\mathbf{z}_{\text{mod}} = (1 + \gamma_t) \odot (\mathbf{z}_{\text{sem}} \cdot \mathbf{g}_t) + \beta_t$$

, where \odot denotes the element-wise Hadamard product. This operation allows the cerebellar module to strictly enforce gain control: for instance, upon detecting a collision (spike in \mathbf{h}_t), the network can suppress the forward velocity encoded in \mathbf{z}_{sem} (via $\gamma_t \approx -1$) and inject a retraction bias (via β_t), effectively rewriting the motor plan in real-time.

4.3.3 Iterative Refinement as a Forward Internal Model

A defining characteristic of cerebellar function is its ability to continuously revise motor intentions based on anticipated sensory feedback. In our model, this predictive correction is operationalized through an *Iterative Refinement Loop*. Upon receiving the updated anticipated state, the module $\text{Refine}(\cdot)$ re-applies the two cerebellar computations introduced in Sections 4.3.1 and 4.3.2 to incrementally adjust the motor latent. We instantiate this via an *Iterative Refinement Loop*. Rather than a single-pass feedforward execution, the module performs K cycles of internal recurrence (set to $K = 2$ in our experiments). In each iteration $k \in \{0, \dots, K-1\}$, the module predicts a tentative action latent, updates the anticipated state evolution, and re-modulates the input. Formally:

$$\mathbf{z}_{\text{mod}}^{(k+1)} \leftarrow \text{Refine}(\mathbf{z}_{\text{mod}}^{(k)}, \mathbf{s}_{t+1})$$

This recursive process acts as a computational “mental simulation,” allowing the agent to minimize the Sim-to-Real gap by pre-correcting for expected dynamical errors (e.g., gravity or friction compensation) prior to actual spinal actuation.

Biological Insight: This architecture instantiates the *Efference Copy* principle. The semantic latent \mathbf{z}_{sem} represents the “intended” movement (efference copy), while \mathbf{h}_t represents the “actual” sensory feedback (re-afference). The FiLM layer computes the discrepancy (sensory prediction error) and applies the necessary correction. This explains why our model exhibits “digital muscle memory”—the ability to adaptively smooth trajectories and reject disturbances without needing to re-invoke the slow, computationally expensive cortical planner.

4.4 Spinal Module: Spiking Residual Dynamics

The Spinal Module serves as the final execution interface, translating the modulated latent intentions \mathbf{z}_{mod} into continuous motor commands \mathbf{a}_t . Implemented on neuromorphic principles, this module is designed to maximize *metabolic efficiency* through event-driven processing and to ensure *trajectory smoothness* via intrinsic neuronal dynamics.

4.4.1 Stateful Leaky Integrate-and-Fire Dynamics

We model the spinal interneurons using the iterative Leaky Integrate-and-Fire (LIF) formalism. Crucially, the network is instantiated with **stateful membrane dynamics**, meaning the membrane potential $u_i^{(l)}$ is strictly preserved across successive time steps rather than being re-initialized at each forward pass. This endows the spinal substrate with an *implicit temporal working memory*, allowing it to encode history-dependent features without requiring explicit recurrent gating units (e.g., LSTMs). For a hidden neuron i in layer l at time step τ , the dynamics evolve according to:

$$u_i^{(l)}[\tau] = \beta u_i^{(l)}[\tau-1] + \sum_j w_{ij} s_j^{(l-1)}[\tau] - s_i^{(l)}[\tau-1] \cdot \vartheta,$$

where $\beta \in (0, 1)$ is the membrane decay factor, w_{ij} is the synaptic weight, $s_j^{(l-1)}[\tau] \in \{0, 1\}$ represents the incoming spike train and ϑ denotes the voltage. The term $u_i^{(l)}[\tau-1]$ represents the *residual potential* carried over from the previous moment, establishing a continuous temporal context.

4.4.2 Deep Spiking Residual Architecture

To enable the learning of complex sensorimotor transformations without signal degradation in deep spiking layers, we structure the spinal module as a Spiking ResNet^{32,33}. By incorporating residual skip connections:

$$\mathbf{x}^{(l+1)} = \mathbf{x}^{(l)} + \text{LIF}(\text{Linear}(\mathbf{x}^{(l)})).$$

We facilitate the direct propagation of gradients and spike rates during training. This architecture mimics the robust signal transmission found in the propriospinal tracts, ensuring that high-level modulation from the cerebellar tier effectively reaches the distal actuation layers.

4.4.3 Continuous Integration for Motor Decoding

A critical challenge in applying SNNs to robotics is bridging the gap between discrete, stochastic spikes and the continuous domain of joint actuation. We resolve this by implementing a **Continuous Integration Protocol** at the output layer³⁴. Unlike hidden interneurons which undergo rapid repolarization (reset) upon spiking, the output motor neurons are configured as **non-resetting integrators**. They continuously accumulate synaptic influx over the simulation window without discharging their potential:

$$\mathbf{a}_t[\tau] = \mathcal{W}_{\text{out}} \cdot \mathbf{u}_{\text{out}}[\tau],$$

where \mathbf{u}_{out} represents the accumulated membrane voltage. This mechanism serves two physiological functions:

1. **Temporal Smoothing:** The integration process acts as a natural low-pass filter, converting high-frequency spike trains into smooth, continuous motor trajectories. This mirrors the biological process of *twitch summation*, where muscles integrate neural drive into continuous force, filtering out neural noise.
2. **Kinematic Consistency:** By maintaining the voltage state, the network naturally enforces temporal consistency in the output action sequence, reducing kinematic jerk and ensuring fluid transitions between control steps.

4.4.4 Surrogate Gradient Learning

To overcome the non-differentiability of the spike generation function $s = \Theta(u - \vartheta)$, we employ a surrogate gradient method for end-to-end training. During the backward pass, the Heaviside step function is approximated by a fast sigmoid function $\sigma(x) = \frac{x}{1+|x|}$, allowing gradients to flow from the continuous action space back through the discrete spinal layers to the cerebellar and cortical modules.

Data Availability

The simulation datasets used in this study are derived from the open-source **LIBERO** and **LIBERO-Plus** benchmarks. The real-world experimental data collected during the current study are available from the corresponding author upon reasonable request.

Code Availability

The code of this paper is available at <https://github.com/guoweiyu/NeuroVLA>.

Acknowledgements

This work was supported in part by the National Key R & D Program of China (Grant No.2023YFF0725001), in part by the National Natural Science Foundation of China (Grant No.92370204), in part by the Guangdong Basic and Applied Basic Research Foundation (Grant No.2023B1515120057), in part by the Education Bureau of Guangzhou.

Author Contributions

W.Y.G. proposed the idea of NeuroVLA, implemented the core codebase, and analyzed the results. P.T.L. designed the real-world experiments, test the performance and discuss the idea. Z.H.T.F.C and Z.Y.C designed the explainable experiments, analyzed the results and discuss the idea. Y.S, Y.K.Y and H.X supervised the literature review, data processing, methodology, analysis, and discussion. Y.D.G, X.H and H.X managed this project.

Figure Legends/Captions

Competing Interests

The authors declare no competing interests.

Inclusion & Ethics Statement

We confirm that this study adheres to all applicable ethical regulations.

References

1. Zitkovich, B., Yu, T., Xu, S., Xu, P., Xiao, T., Xia, F., Wu, J., Wohlhart, P., Welker, S., Wahid, A. and others. Rt-2: Vision-language-action models transfer web knowledge to robotic control. In *Conference on Robot Learning*, 2165–2183 (2023).
2. Kim, M. J., Pertsch, K., Karamcheti, S., Xiao, T., Balakrishna, A., Nair, S., Rafailov, R., Foster, E. P., Sanketi, P. R., Vuong, Q., Kollar, T., Burchfiel, B., Tedrake, R., Sadigh, D., Levine, S., Liang, P., and Finn, C. OpenVLA: An Open-Source Vision-Language-Action Model. In *8th Annual Conference on Robot Learning* (2024).
3. Scott, S. H. Optimal feedback control and the neural basis of volitional movement. *Nature Reviews Neuroscience* **5**, 532–546 (2004).
4. Todorov, E. Optimality principles in sensorimotor control. *Nature Neuroscience* **7**, 907–915 (2004).

5. K. Doya, "What are the computations of the cerebellum, the basal ganglia and the cerebral cortex?" in *Elsevier Science Ltd.*, 1999.
6. M. Ito, "Control of mental activities by internal models in the cerebellum," *Nature Reviews Neuroscience*, vol. 9, no. 4, pp. 304–313, 2008. doi:10.1006/jsvi.1999.2518.
7. S. Vahdat, O. Lungu, J. Cohen-Adad, V. Marchand-Pauvert, H. Benali, and J. Doyon, "Simultaneous Brain–Cervical Cord fMRI Reveals Intrinsic Spinal Cord Plasticity during Motor Sequence Learning," *PLoS Biology*, vol. 13, 2015. doi:10.1371/journal.pbio.1002186.
8. Vahdat, S., Lungu, O., Cohen-Adad, J., Marchand-Pauvert, V., Benali, H., Doyon, J. Simultaneous brain–cervical cord fMRI reveals intrinsic spinal cord plasticity during motor sequence learning. *PLoS Biology* **13**, e1002186 (2015).
9. K. Roy, A. Jaiswal, and P. Panda, "Towards spike-based machine intelligence with neuromorphic computing," *Nature*, vol. 575, no. 7784, pp. 607–617, 2019. doi:10.1038/s41586-019-1677-2.
10. Bartolozzi, C., Indiveri, G., Donati, E. Embodied neuromorphic intelligence. *Nature Communications* **13**, 1024 (2022).
11. Li, J., Li, D., Savarese, S., Hoi, S. BLIP-2: Bootstrapping language-image pre-training with frozen image encoders and large language models. *International Conference on Machine Learning*, 19730–19742 (2023).
12. Garrido, J., Luque, N., D'Angelo, E., Ros, E. Distributed cerebellar plasticity implements adaptable gain control in a manipulation task: A closed-loop robotic simulation. *Frontiers in Neural Circuits* **7**, 159 (2013).
13. Black, K. *et al.* $\pi_{0.5}$: A vision-language-action model with open-world generalization. *9th Annual Conference on Robot Learning* (2025).
14. Zhao, Q., Zhang, L., Zhang, H., Jiang, H., Cui, K., Wu, Z., Liu, J., Zhao, M., Tian, F., Hu, B. LSNN model: A lightweight spiking neural network-based depression classification model for wearable EEG sensors. *IEEE Transactions on Mobile Computing* (2025).
15. Kim, M. J., Finn, C., and Liang, P. Fine-Tuning Vision-Language-Action Models: Optimizing Speed and Success. *ArXiv abs/2502.19645* (2025).
16. Cen, J., Yu, C., Yuan, H., Jiang, Y., Huang, S., Guo, J., Li, X., Song, Y., Luo, H., Wang, F., Zhao, D., and Chen, H. WorldVLA: Towards Autoregressive Action World Model. *ArXiv abs/2506.21539* (2025).
17. Wang, Y.-Q., Li, X., Wang, W., Zhang, J., Li, Y., Chen, Y., Wang, X., and Zhang, Z. Unified Vision-Language-Action Model. *ArXiv abs/2506.19850* (2025).
18. Liu, B., Zhu, Y., Gao, C., Feng, Y., Liu, Q., Zhu, Y., and Stone, P. Libero: Benchmarking knowledge transfer for lifelong robot learning. *Advances in Neural Information Processing Systems* **36**, 44776–44791 (2023).
19. Li, J., Li, D., Savarese, S., and Hoi, S. C. H. BLIP-2: Bootstrapping Language-Image Pre-training with Frozen Image Encoders and Large Language Models. In *International Conference on Machine Learning* (2023).
20. Feldman, D. E. The spike-timing dependence of plasticity. *Neuron* **75**, 556–571 (2012).
21. Caporale, N. and Dan, Y. Spike timing–dependent plasticity: a Hebbian learning rule. *Annu. Rev. Neurosci.* **31**, 25–46 (2008).
22. Neftci, E. O., Mostafa, H., and Zenke, F. Surrogate gradient learning in spiking neural networks: Bringing the power of gradient-based optimization to spiking neural networks. *IEEE Signal Processing Magazine* **36**, 51–63 (2019).
23. Perez, E., Strub, F., De Vries, H., Dumoulin, V., and Courville, A. FiLM: Visual reasoning with a general conditioning layer. In *Proceedings of the AAAI conference on artificial intelligence* **32**, (2018).
24. Abbott, L. F. Lapicque's introduction of the integrate-and-fire model neuron (1907). *Brain research bulletin* **50**, 303–304 (1999).
25. Akopyan, F., Sawada, J., Cassidy, A., Alvarez-Icaza, R., Arthur, J., Merolla, P., Imam, N., Nakamura, Y., Datta, P., Nam, G.-J., *et al.* Truenorth: Design and tool flow of a 65 mw 1 million neuron programmable neurosynaptic chip. *IEEE transactions on computer-aided design of integrated circuits and systems* **34**, 1537–1557 (2015).
26. Davies, M., Srinivasa, N., Lin, T.-H., Chinya, G., Cao, Y., Choday, S. H., Dimou, G., Joshi, P., Imam, N., Jain, S., *et al.* Loihi: A neuromorphic manycore processor with on-chip learning. *Ieee Micro* **38**, 82–99 (2018).
27. Qiu, Z., Wang, Z., Zheng, B., Huang, Z., Wen, K., Yang, S., Men, R., Yu, L., Huang, F., Huang, S., Liu, D., Zhou, J., and Lin, J. Gated Attention for Large Language Models: Non-linearity, Sparsity, and Attention-Sink-Free. In *The Thirty-ninth Annual Conference on Neural Information Processing Systems* (2025).

28. Chung, J., Gulcehre, C., Cho, K., and Bengio, Y. Empirical evaluation of gated recurrent neural networks on sequence modeling. *arXiv preprint arXiv:1412.3555* (2014).
29. Pei, J., Deng, L., Song, S., Zhao, M., Zhang, Y., Wu, S., Wang, G., Zou, Z., Wu, Z., He, W., et al. Towards artificial general intelligence with hybrid Tianjic chip architecture. *Nature* **572**, 106–111 (2019).
30. Lauri, M., Hsu, D., and Pajarin, J. Partially observable markov decision processes in robotics: A survey. *IEEE Transactions on Robotics* **39**, 21–40 (2022).
31. Fei, S., Wang, S., Shi, J., Dai, Z., Cai, J., Qian, P., Ji, L., He, X., Zhang, S., Fei, Z. and others. Libero-plus: In-depth robustness analysis of vision-language-action models. *arXiv preprint arXiv:2510.13626* (2025).
32. Fang, W., Yu, Z., Chen, Y., Huang, T., Masquelier, T., and Tian, Y. Deep residual learning in spiking neural networks. *Advances in Neural Information Processing Systems* **34**, 21056–21069 (2021).
33. Hu, Y., Tang, H., and Pan, G. Spiking deep residual networks. *IEEE Transactions on Neural Networks and Learning Systems* **34**, 5200–5205 (2021).
34. Guo, W., Sun, Y., Xu, Y., Qiao, Z., Yang, Y., and Xiong, H. SpGesture: Source-Free Domain-adaptive sEMG-based Gesture Recognition with Jaccard Attentive Spiking Neural Network. *Advances in Neural Information Processing Systems* **37**, 36717–36747 (2024).
35. Rao, A., Plank, P., Wild, A., and Maass, W. A long short-term memory for AI applications in spike-based neuromorphic hardware. *Nature Machine Intelligence* **4**, 467–479 (2022).
36. Rathi, N., Chakraborty, I., Kosta, A., Sengupta, A., Ankit, A., Panda, P., and Roy, K. Exploring Neuromorphic Computing Based on Spiking Neural Networks: Algorithms to Hardware. *ACM Computing Surveys* **55**, 1–49 (2022).
37. Liu, Y., Chen, W., Bai, Y., Liang, X., Li, G., Gao, W., Lin, L. Aligning cyber space with physical world: A comprehensive survey on embodied AI. *IEEE/ASME Transactions on Mechatronics*, 1–22 (2025).
38. Bruel, A., Abadía, I., Collin, T., Sakr, I., Lorach, H., Luque, N. R., Ros, E., Ijspeert, A. The spinal cord facilitates cerebellar upper limb motor learning and control; inputs from neuromusculoskeletal simulation. *PLOS Computational Biology* **20**, e1011008 (2024).
39. H. Lorach, A. Gálvez, V. Spagnolo, F. Martel, S. Karakas, N. Interling, M. Vat, O. Fairve, C. Harte, S. Komi, J. Ravier, T. Collin, L. Coquoz, I. Sakr, E. Baaklini, S. D. Hernandez-Charpak, G. Dumont, R. Buschman, N. Buse, T. Denison, I. V. van Nes, L. Asboth, A. Watrin, L. Struber, F. Sauter-Starace, L. Langar, V. Auboiron, S. Carda, S. Chabardès, T. Aksanova, R. Demesmaeker, G. Charvet, J. Bloch, and G. Courtine, “Walking naturally after spinal cord injury using a brain-spine interface,” *Nature*, vol. 618, pp. 126–133, 2023.
40. Niu, Z., Zhong, G., Yu, H. A review on the attention mechanism of deep learning. *Neurocomputing* **452**, 48–62 (2021).
41. K. Kawaharazuka *et al.*, “Vision-Language-Action Models for Robotics: A Review Towards Real-World Applications,” *IEEE Access*, 2025.
42. Yang, S., Wang, J., Zhang, N., Deng, B., Pang, Y., Azghadi, M. CerebelluMorphic: Large-scale neuromorphic model and architecture for supervised motor learning. *IEEE Transactions on Neural Networks and Learning Systems* **33**, 4398–4412 (2022).
43. Black, K., Galliker, M. Y., Levine, S. Real-time execution of action chunking flow policies. *The Thirty-ninth Annual Conference on Neural Information Processing Systems* (2025).
44. Suárez, L. E., Richards, B. A., Lajoie, G., Misic, B. Learning function from structure in neuromorphic networks. *Nature Machine Intelligence* **3**, 771–786 (2021).